Anthropogenic chloroform emissions from China drive changes in global emissions

Minde An[1,2,3], Luke M. Western[2,4], Jianxin Hu[1], Bo Yao[5,6*], Jens Mühle[7], Anita L. Ganesan[8], Ronald G. Prinn[3], Paul B. Krummel[9], Ryan Hossaini[10], Xuekun Fang[11], Simon O'Doherty[2], Ray F. Weiss[7], Dickon Young[2], Matthew Rigby[2*]*

1 College of Environmental Sciences and Engineering, Peking University, Beijing, 100871, China

2 School of Chemistry, University of Bristol, Bristol, BS8 1TS, UK

3 Center for Global Change Science, Massachusetts Institute of Technology, Cambridge, MA, 02139, USA

4 Global Monitoring Laboratory, National Oceanic and Atmospheric Administration, Boulder, CO, 80305, USA

5 Department of Atmospheric and Oceanic Sciences & Institute of Atmospheric Sciences, Fudan University, Shanghai, 200438, China

6 Meteorological Observation Centre of China Meteorological Administration (MOC/CMA), Beijing, 100081, China

7 Scripps Institution of Oceanography, University of California San Diego, La Jolla, CA, 92093, USA

8 School of Geographical Sciences, University of Bristol, Bristol, BS8 1SS, UK

9 Climate Science Centre, CSIRO Oceans and Atmosphere, Aspendale, Victoria, VIC 3195, Australia

10 Lancaster Environment Centre, Lancaster University, Lancaster, LA1 4YQ, UK

11 College of Environmental & Resource Sciences, Zhejiang University, Zhejiang, 310058, China

*** Corresponding authors**:

Jianxin Hu: jianxin@pku.edu.cn; Bo Yao: yaobo@fudan.edu.cn; Matthew Rigby: Matt.Rigby@bristol.ac.uk

Keywords: chloroform; ozone layer depletion; Montreal Protocol; emissions; very short-lived ozone-depleting substances

Abstract

Emissions of chloroform ($CHCl_3$), a short-lived halogenated substance not currently controlled under the Montreal Protocol on Substances that Deplete the Ozone Layer, are offsetting some of the achievements of the Montreal Protocol. In this study, emissions of $CHCl_3$ from China were derived by atmospheric measurement-based "top-down" inverse modelling and a sector-based "bottom-up" inventory method. Top-down $CHCl_3$ emissions grew from 78 (72-83) Gg yr^{-1} in 2011 to a maximum of 193 (178-204) Gg yr^{-1} in 2017, followed by a decrease to 147 (138-154) Gg yr^{-1} in 2018, after which emissions remained relatively constant through 2020. The changes in emissions from China could explain all the global changes during the study period. The $CHCl_3$ emissions in China were dominated by anthropogenic sources, such as by-product emissions during disinfection and leakage from chloromethane industries. Had emissions continued to grow at the rate observed up to 2017, a delay of several years in Antarctic ozone layer recovery could have occurred. However, this delay will be largely avoided if global $CHCl_3$ emissions remain relatively constant in the future, as they have between 2018 and 2020.

Synopsis: A recent increase and subsequent decrease in emissions of ozone-depleting chloroform is inferred in China using atmospheric measurements.

Introduction

Due to the phase-down of production and consumption of long-lived ozone depleting substances such as chlorofluorocarbons (CFCs), halons, and hydrochlorofluorocarbons (HCFCs) under the Montreal Protocol on Substances that Deplete the Ozone layer, the burden of stratospheric chlorine and bromine is declining and the Antarctic ozone hole is showing signs of recovery[1,2]. Previous studies have identified that halogenated very short-lived substances (VSLSs), defined as species with a total atmospheric lifetime shorter than 6 months, play an increasing role in stratospheric ozone depletion[3,4], especially if they are emitted from regions with rapid transport pathways to the stratosphere such as East and South Asia[5-7]. The impact of VSLSs on ozone layer depletion is more prominent if considered in terms of the integrated ozone depletion (IOD)[8] compared to the traditional metrics such as ozone depletion potential (ODP).

Chloroform ($CHCl_3$) is the second most abundant chlorine-containing VSLSs, with a lifetime of ~6 months[2]. There was substantial growth in the measured global atmospheric mole fractions of $CHCl_3$ and a rapid increase in global $CHCl_3$ emissions between 2010-2015[9]. If the growth of the atmospheric abundance of $CHCl_3$ were to have continued at the rate observed between 2010 and 2015, it could delay Antarctic stratospheric ozone layer recovery by several years[9], comparable to the impact from recent unexpected CFC-11 emissions between 2013 and 2019[10,11]. However, global $CHCl_3$ emissions and mole fractions have recently been found to have decreased after reaching a maximum in 2017[2].

Given the growing impact of VSLSs on ozone layer depletion compared to ozone depleting substances controlled under the Montreal Protocol, it is important to better understand the magnitude and distribution of their sources. The global increase in $CHCl_3$ emissions between 2010 and 2015 was attributed primarily to anthropogenic emissions in China[9], but the contribution of individual source sectors was not investigated in detail. Most of the $CHCl_3$ produced in China is thought to be consumed as a feedstock and converted to HCFC-22[12], where only a few percent of the feedstock are thought to leak to the atmosphere[13,14]. Several disinfection processes may lead to by-product emissions of $CHCl_3$ via haloform reactions[15,16], but their contribution has not been quantified. In addition to anthropogenic sources, natural sources of $CHCl_3$ including ocean emissions and terrestrial soil emissions are also significant worldwide (accounting for more than 50% of the global emissions)[16-19], and similar natural processes in China may contribute substantially to $CHCl_3$ emissions. To date, there has been no sector-based bottom-up inventory for $CHCl_3$ emissions in China, and thus little quantitative understanding of the potential source sectors responsible for the increase in $CHCl_3$ emissions. The cause of the global emission decrease after 2017 has not previously been identified.

Quantifying $CHCl_3$ emissions from China is important considering its predominant role in the global increase between 2010-2015[9] and the rapid upward transport to the stratosphere of emissions from East Asia compared to those from other industrialized areas such as mid-latitude Europe or North America[6,20]. In this study, we provide a time-series of $CHCl_3$ emissions from China (defined as the Chinese mainland, excluding

Hong Kong, Macao and ocean areas) using sector-based "bottom-up" information (2006-2020) and atmospheric measurement-based "top-down" methods (2011-2020), to constrain $CHCl_3$ emissions and examine the potential sources driving the apparent trends. Previous top-down emissions estimates were localized to eastern China and were derived from measurements of atmospheric mole fractions made outside of China[9], while the top-down estimation in this study focuses on emissions from the whole of China, derived from long-term measurements from a network of nine sites within China. The results in this study combined with previously reported global emissions allow a better understanding of global-scale changes in emissions of $CHCl_3$ and their potential impact on the ozone layer.

Methods

Site description and measurement

The regional top-down inversion of $CHCl_3$ emissions from China used measurements at nine sites from the China Meteorological Administration (CMA): Akedala (AKD, 47.10° N 87.97° E), Lin'an (LAN, 30.30° N 119.73° E), Longfengshan (LFS, 44.73° N 127.60° E), Jiangjin (JGJ, 29.15° N 106.15° E), Jinsha (JSA, 29.64° N 114.21° E), Shangdianzi (SDZ, 40.65° N 117.21° E), Mt. Waliguan (WLG, 36.29° N 100.90° E), Shangri-La (XGL, 28.01° N 99.44° E), and Xinfeng (XFG, 24.08° N 114.17° E). These sites provide measurements with sensitivity to emissions sources across China (Supplementary Fig. S1). All the sites are far (typically 10s to 100s of km) from heavily industrialized areas, thus minimizing the influence of very localized emissions sources

on the measurements. A summary of the sampling period and frequency at each site is provided in Supplementary Table S1. Ambient air samples were collected weekly in flasks at AKD, LFS, JSA, SDZ, WLG, XGL and XFG, and daily from JGJ. At LAN, the sampling frequency was weekly before 2019 and daily thereafter. The sampling time for the flasks was around 2 pm local time when the height of boundary layer was highest, except for WLG where the samples were collected at 8 am local time due to its unique topography, to ensure horizontal winds bringing downslope airflow. All flask air samples were sent to the CMA Beijing lab for analysis. In addition to the flask samplings above, there were also high-frequency in-situ measurements at SDZ during the study period. More detailed information about the measurement sites and sampling processes are provided in previous papers[21-23].

Two instruments were used in this study to analyze the mole fractions of $CHCl_3$ in the air samples: an AGAGE (Advanced Global Atmospheric Gases Experiment) 'Medusa' gas chromatographic system with mass spectrometric detector (GC/MS)[24,25], and a 2-channel gas chromatograph with electron-capture detector (GC-ECD)[26]. All the flask samples were analyzed by the GC/MS system at CMA. At SDZ, ambient air was sampled and analyzed every 2 hours by the GC/MS system and every 80 minutes by the GC-ECD system. The analysis of the flask samples follows the same process as the in-situ measurement. Every air sample was bracketed by an analysis of the working standard to calibrate the drift in the system. All $CHCl_3$ measurements are reported on the SIO-98 calibration scale[27]. Measurement precisions were estimated at 3.4%, 0.6% and 1.5% for the in-situ GC-ECD, in-situ GC/MS at SDZ and flask samples,

respectively, where the precision for flask sampling was estimated as the typical standard deviation of the two parallel detections. All raw measurements are in Supplementary Data File 1. At SDZ, the flask sampling and in-situ measurement show great consistency (Supplementary Fig. S2). If both GC/MS and GC-ECD SDZ in-situ measurements were available in a specific year, the measurements using GC/MS were used in the inversion unless the GC/MS instrument was not operational in that year, in which case the GC-ECD measurements were used. All in-situ measurements from SDZ were averaged over a period of 24 hours in the inversion framework. In addition, a "local influence" filter was applied to the daily samples at JGJ, LAN and in-situ measurements at SDZ to remove measurements where the signal is mostly influenced by emissions sources close to the sites (if they exist), which are poorly represented in the inversion framework. We filtered out observations where the sum of the sensitivities of the observation to emissions in the nearest 25 grid cells surrounding the measurement site in the atmospheric transport model was more than 10% of the total sensitivity (see next section for atmospheric transport model and definition of grid cells). After re-sampling and filtering, a total of 4030 processed measurements were included in the inversions to estimate emissions from China.

Regional inversion framework

A hierarchical Bayesian inference method[28-31] coupled with the UK Met Office Numerical Atmospheric-dispersion Modelling Environment (NAME)[32] was utilized in this study to derive regional emissions of $CHCl_3$ from China and has been described in

156 detail in previous studies[21,33,34]. Here we provide a brief overview about the general
157 framework, and several updates including the changes in a priori emission information
158 and uncertainties.

159 The observations from the CMA network were combined with sensitivities of each
160 measurement to the emissions from each grid within a regional domain, and sensitivities
161 of each measurement to the mole fraction at the domain boundary (boundary
162 conditions). The regional domain in this study was bounded at 5º S, 74º N and 55º E,
163 192º E. The grid cells were 0.352º in longitude and 0.234º in latitude. The sensitivities
164 to both emissions and boundary conditions were modelled using the Lagrangian
165 Particle Dispersion Model, NAME[32], driven by meteorological fields from the UK Met
166 Office Unified Model[35]. In NAME, 20,000 tracer particles were released per hour from
167 the sampling location within a ±10 m vertical window and the model was run
168 backwards in time for 30 days. Particles in the lowest 40 m of the atmosphere were
169 regarded as having interacted with surface emissions[28], and sensitivities to surface
170 emissions were integrated over the 30-day simulations. Locations of the particles
171 leaving the domain were also integrated to calculate boundary conditions, or
172 background mole fractions. The mole fraction enhancements above the backgrounds
173 were used to derive regional emissions within the domain. Chemical loss during
174 transport was not considered, as a previous study showed that the chemical loss plays
175 only a minor role in the regional inversion for $CHCl_3$ (<1% of the derived emissions,
176 which is small compared to other estimated uncertainties in the inversion)[9].

In the hierarchical Bayesian inference framework, the emissions, boundary conditions and the model-measurement uncertainties were sampled using a Markov Chain Monte-Carlo (MCMC) method, constructed by a No-U-Turn sampler[36] and a slice sampler[37]. The MCMC chain used 2.5×10^5 steps, and the first 5×10^4 steps from the chain were discarded. Prior to sampling, 1.25×10^5 tuning steps were run. The mean and 68% uncertainty interval from the posteriori distribution were calculated as the reported emissions and their uncertainties. In the Bayesian inference, the a priori estimate for emissions of $CHCl_3$ from China was obtained from the bottom-up inventory in this study (see next section). A total of 80% of the a priori emissions were distributed in space by a function of nightlight density data from NOAA DMSP-OLS (Defense Meteorological Satellite Program-Operational Line-Scan System, https://ngdc.noaa.gov/eog/data/web_data/v4composites/) where nightlight values below 0.5 were treated as zero. The remaining 20% were allocated uniformly to the grids with zero nightlight values to simulate natural sources. The a priori estimate for mole fractions at the domain boundaries come from the 3D TOMCAT model[38].

The grid cells in the regional domain were aggregated into 150 regions (defined as "basis functions") by a quadtree algorithm[39], in which emissions were estimated in the inversion framework. The parameters estimated in the inversion were scaling factors to the a priori emissions across the 150 regions, scaling factors to the boundary conditions on each horizontal boundary and the model error. These were solved for annually. The scaling factors for the a priori emissions and a priori boundary conditions were sampled from a log-normal prior distribution with mean and standard deviation of 1, which can

constrain the posteriori values to an appropriate magnitude and avoid negative values. The model uncertainty was solved using a uniform distribution following An et al.[21]. When averaging the SDZ in-situ data into 24 hours, an averaging error was added to the uncertainty of the final data which was the quadratic mean of the raw data uncertainties. The uncertainties for SDZ in-situ data and SDZ flask data were solved separately in the inversion.

Diagnosis of the top-down emissions results from the inverse modelling framework

To validate the emission results, several sensitivity tests were conducted, including inversions using different a priori emission magnitudes (Supplementary Fig. S3a), different a priori emission probability distributions (Supplementary Fig. S3b), different sites (Supplementary Fig. S4), different number of measurements (Supplementary Fig. S5), different filter settings (Supplementary Fig. S6a) and different basis functions (Supplementary Fig. S6b). All these tests show good consistency in magnitudes and inter-annual variabilities of $CHCl_3$ emissions in China.

In addition, an "error reduction" term was defined in this study to evaluate the convergence of the Markov Chain Monte-Carlo sampling in the Bayesian framework, which can be described by equation (1),

$$ER = 1 - \frac{HPD_{68,post}}{HPD_{68,prior}} \quad (1)$$

where ER is the error reduction term in a specific region; $HPD_{68,post}$ is the 68% uncertainty interval of the posteriori samples from the Markov Chain, defined as the

highest posteriori density; $HPD_{68,prior}$ is the corresponding uncertainty interval for the a priori emissions. The error reductions for emissions in China and in all regions in each year are provided in Supplementary Data file 2. The error reductions for the total emissions in China are all above 80% over the study period, which means the Markov Chain sampler substantially reduces the uncertainty of the fairly uninformative log-normal a priori distribution and reaches a good convergence.

The root mean square error (RMSE) term was also used in this study to evaluate the fit of the modelled observations using a prescribed emissions to the real observations, which can be calculated by equation (2),

$$RMSE = \sqrt{\frac{\sum(y_{mod} - y_{meas})^2}{N}} \quad (2)$$

where $\boldsymbol{y_{mod}}$ is the modelled observations using the a priori emissions or posteriori emissions; $\boldsymbol{y_{meas}}$ is the real observations; $\boldsymbol{N}$ is the number of observations. We calculate the improvement in the RMSEs for all years and all sites by comparing results obtained using the posteriori emissions with those using a priori emissions, by equation (3),

$$improvement = 1 - \frac{RMSE_{post}}{RMSE_{prior}} \quad (3)$$

where $RMSE_{post}$ is the RMSE using posteriori emissions, and $RMSE_{prior}$ is the RMSE using a priori emissions. The calculated RMSE improvements are shown in Supplementary Table S2. After the Markov Chain sampling, the posteriori emissions provide a better fit to the observations than the a priori emissions.

Bottom-up inventory for $CHCl_3$ in China

The bottom-up inventory considers both anthropogenic sources and natural sources for $CHCl_3$ emissions in China. The categories (source sectors) of anthropogenic emissions in the inventory are shown in Fig. 1. Anthropogenic emissions of $CHCl_3$ in China mainly originate from emissions or leakages during intentional consumption or production of $CHCl_3$ (defined as intended emissions in this study), and unintended emissions of $CHCl_3$ during processes where $CHCl_3$ is emitted as an unwanted by-product (defined as by-product emissions in this study). The intended emissions include emissions from (a) production leakage, (b) feedstock use leakage and (c) solvent use in the pharmaceutical industry. The by-product emissions sector is a considerable source of $CHCl_3$ emissions, where $CHCl_3$ may be formed as a disinfectant by-product through a haloform reaction, be produced during combustion or in anaerobic processes associated with methane[15,16]. In this study, the by-product sector includes (d) the pulp and paper industry, (e-g) water treatment, (h) biomass burning, (i) coal combustion, (j) waste incineration, (k) landfill, and (l) livestock.

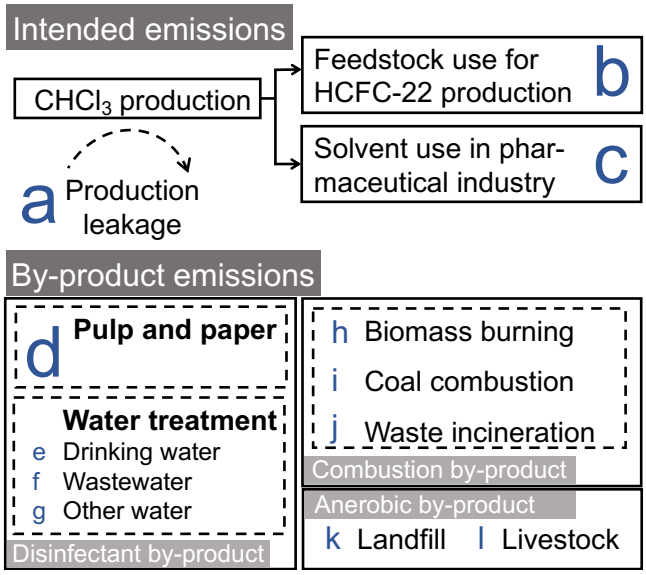

Fig. 1 Categories of source sectors for anthropogenic $CHCl_3$ emissions in China considered in the bottom-up inventory. *The anthropogenic emissions include two categories, intended emissions (sector a-c), which are the emissions or leakages of $CHCl_3$ during its intentional consumption or production, and by-product emissions (sector d-l), which are the emissions of $CHCl_3$ as an unwanted by-product in some processes. The details for each sector can be found in the Methods. The natural emissions, sector (m), are not shown in this diagram.*

The emissions in each sector, unless specified otherwise, were estimated by multiplying activity data for each sector by the corresponding emission factors, as shown by equation (4),

$$E_i = Ef_i \times A_i \quad (4)$$

where E_i is the emission of $CHCl_3$ in sector i in a specific year; Ef_i is the emission factor(s) in that sector; and A_i is the corresponding activity data in the sector. All activity data and emission factors are listed in Supplementary Table S3-5.

The total $CHCl_3$ production data in 2006-2010 and 2013-2020 were taken from the China Chlor-Alkali Industry Association (CCAIA)[12]. CCAIA also provides total chloromethane production data in 2006-2020[12]. There is no data on $CHCl_3$ production in 2011-2012 and so these data were estimated by multiplying the total chloromethane production in 2011/2012, obtained from CCAIA[12], by the percentage of $CHCl_3$ production to total chloromethane production, averaged over the year before and after the missing data (i.e., 2010 and 2013). The production data were used as activity data in sector (a). The import and export data were taken from China Customs Statistics Yearbook or CCAIA[12,40]. The consumption data were calculated as production plus import minus export.

For production leakage, sector (a), we applied 0.5-4% as a range of leakage rates (emission factor) in this study to account for the uncertainties in emissions during production or other relevant processes such as fugitive emissions during transport and storage. The 0.5% leakage rate is recommended by IPCC 2000 guidelines[41] for substitutes of ozone depleting substances and 4% is recommended by IPCC 2019 guidelines[42] for fluorochemicals. Much higher emission factors potentially exists for this sector[42,43] and were tested in the Supplementary Fig. S7.

For sector (b), all feedstock use of $CHCl_3$ in China is for production of HCFC-22, which may be used directly or further used as feedstock for fluorinated polymers. In this sector, the amount of $CHCl_3$ used for HCFC-22 production (i.e., activity data) was derived from annual HCFC-22 production[44] and mass balance of $CHCl_3$ to HCFC-22

290 conversion, with a conversion efficiency of 95% (following consultation with industry
291 experts; this value is similar to values previously reported for production of HFC-32[14]).
292 We assumed 0.5% as the leakage rate of $CHCl_3$ (emission factor) during feedstock use
293 for HCFC-22 production, similar to leakage rates of other major chloromethanes during
294 feedstock use reported in previous studies[13,14,21].

295 For sector (c), the majority of $CHCl_3$ used in other industrial processes, except for its
296 feedstock use for HCFC-22 production, is as a solvent in the pharmaceutical
297 industry[12,15]. Thus, in this study, the $CHCl_3$ emissions from other industrial processes
298 only refer to emissions during solvent use in pharmaceutical manufacturing. About 8-
299 10% of $CHCl_3$ consumption was used as a solvent in the pharmaceutical industry[12],
300 which is adopted as the activity data in this sector (c). We assumed an emission factor
301 of 5-16% in sector (c)[15,21,45].

302 In the pulp and paper industry, sector (d), $CHCl_3$ could be produced as a by-product
303 during disinfecting or bleaching processes. The activity data for sector (d) was the paper
304 produced each year in China, taken from the China Statistical Yearbook[46], and the
305 emission factors were 5.3×10^{-5} to 4.54×10^{-4} g $CHCl_3$ per gram of paper produced[15,19,45].

306 The water treatment sector emits $CHCl_3$ during disinfection in drinking water treatment
307 (sector (e)), wastewater treatment (sector (f)), and other water treatment (sector (g)).
308 The amount of drinking water and wastewater treated each year was obtained from the
309 China Urban-Rural Construction Statistical Yearbook[47] and used as the activity data in
310 these sectors. The emission factors were 4.1×10^{-5} and 1.4×10^{-5} g L^{-1} for drinking water

311 treatment and wastewater treatment, respectively[45]. The emissions from other water
312 treatment were estimated to be 70% of the sum of emissions from drinking water
313 treatment and wastewater treatment[15].

314 For sector (h), the emissions of $CHCl_3$ from biomass burning were estimated by the
315 emission ratio of $CHCl_3$/CO and $CHCl_3/CO_2$[48]. The reference emissions of CO and CO_2
316 from biomass burning were obtained from a previous study[49], where the emissions of
317 the two substances after 2015 were extrapolated linearly from the data in 2008-2014.
318 The average of the two derived emissions based on CO and CO_2, respectively, in each
319 year was adopted as the emissions of $CHCl_3$ from biomass burning.

320 For sector (i), the amount of coal combusted was obtained from the China Energy
321 Statistical Yearbook[50] as the activity data, and the emission factor of $CHCl_3$ from coal
322 combustion was 2.95×10^{-8} g $CHCl_3$ per gram of coal burned[51].

323 For sector (j) and (k), the quantity of waste incineration and waste landfill were obtained
324 from the China Urban-Rural Construction Statistical Yearbook[47], used as the activity
325 data in the sectors, and the emission factors for the two sectors were 3.51×10^{-8} to 5.39
326 $\times 10^{-7}$ g $CHCl_3$ per gram of waste incinerated (obtained from USEPA[51]), and 6.33×10^{-7}
327 g $CHCl_3$ per gram of landfill (averaged from Liu et al.[52]), respectively.

328 For sector (l), the emissions of $CHCl_3$ from livestock were estimated by the emissions
329 of CH_4 from livestock averaged from different studies[53-55], and the emission ratio of 2
330 $\times 10^{-5}$ g $CHCl_3$ per gram of CH_4 produced[15,16]. The emissions of CH_4 from Chang et al.[55]
331 in 2019-2020 were extrapolated linearly by available data in all other years.

Natural sources contribute to ~50-90% of the global $CHCl_3$ emissions reported in previous studies[16-19]. For the natural $CHCl_3$ emissions in China, the sector (m), only terrestrial natural emissions are considered as there is no ocean area involved for China in this study. The terrestrial natural emissions of $CHCl_3$ include emissions from several land types such as peatland emissions[56], forest soil emissions[57] or rice field emissions[58] (rice emissions are anthropogenic but categorized into terrestrial natural emissions in this study for ease of calculation), and the real release rate of $CHCl_3$ over different terrestrial land types may be highly variable[16,57,58]. Here, we used a range of 4-13 $\mu g\ m^{-2}\ d^{-1}$ measured by a reported chamber study[59] as the $CHCl_3$ release rate from soil, which lies within the same magnitude as several field studies[16]. The rate was applied to the total land area of China of ~$9.6 \times 10^{12}\ m^2$, to approximate $CHCl_3$ emissions from a range of soil processes. Terrestrial $CHCl_3$ emissions in China are subject to large uncertainty due to the various and uncertain land type in China. A more precise examination of natural $CHCl_3$ sources in China could be possible in further studies.

All the statistical data obtained directly from the statistical yearbooks and the reference emissions obtained from other studies, which were used to quantify the activity data in each sector, were assumed to have a normal distribution with 5% uncertainty. If multiple values or a value range was given for a specific variable, a uniform distribution would be adopted to calculate the uncertainty. A Monte-Carlo method with 10,000 samples was used to estimate the emissions and their uncertainties (68% interval).

Results

Top-down emissions of $CHCl_3$ in China and contribution to global emissions

Emissions of $CHCl_3$ in China during 2011-2020 were derived from measurements of atmospheric mole fraction from nine sites within China (see Methods, measurement data shown in Supplementary Fig. S8 and Supplementary Data file 1). The model simulation using the derived emissions provide a closer fit to the observations compared to the simulation using the a priori emissions, in terms of RMSE (see Supplementary Table S2). Figure 2a shows that emissions in China increased from 78 (72-83) Gg yr^{-1} in 2011 to 193 (178-204) Gg yr^{-1} in 2017, continuing the increase in $CHCl_3$ emissions from eastern China previously reported through 2015[9]. A decrease in $CHCl_3$ emissions occurred after the maximum in 2017, reaching 147 (138-154) Gg yr^{-1} in 2018. Emissions were approximately constant during 2018-2020. The derived emissions and their trends are generally insensitive to the choice of a priori emissions magnitude (Supplementary Fig. S3a), the choice of probability distribution in the inversion framework (Supplementary Fig. S3b), the choice of Chinese measurement datasets (Supplementary Fig. S4-5), or different methods of filtering the data and assigning basis functions (Supplementary Fig. S6).

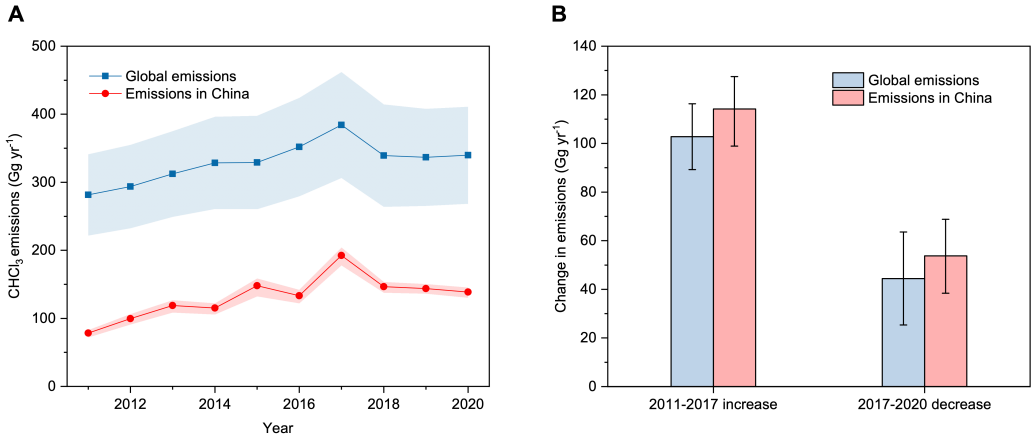

Fig. 2 Annual $CHCl_3$ emissions in China and global emissions. ***(A)*** *A comparison of $CHCl_3$ emissions in China with global emissions. The annual emissions in China can be found in Supplementary Data file 3. The annual global emissions are derived from Laube and Tegtmeier et al.*[2] *using the AGAGE global background data.* ***(B)*** *The increase in the global emissions and emissions in China between 2011 and 2017 (i.e., 2017 minus 2011) and the decrease between 2017 and 2020 (i.e., 2017 minus 2020). The uncertainties, indicated by shading in* ***(A)*** *and error bars in* ***(B),*** *are 1-sigma or the 68% uncertainty interval.*

The derived top-down emissions from China play an important role in the global emissions, accounting for ~25-50% of the global total over 2011-2020, with a maximum proportion of the global total of ~50% in 2017 (Fig. 2a). The emissions in China show a similar trend to the global emissions, which both reached a maximum in 2017, followed by a decrease and then a plateau between 2018 and 2020. The pre-2017 increase (difference between the years 2011 and 2017) and the post-2017 decrease (difference between the years 2017 and 2020) of emissions in China are of the same

magnitude, or even larger, than the global change in the same period (Fig. 2b). These coincident emission trends indicate that the changes of $CHCl_3$ emissions from China may be the dominant contributor to global emission changes during this period.

Anthropogenic emission sources are indicated to be the dominant driver for the emission changes globally and in China, as it is not possible to explain the entire variation in global emissions by changes from terrestrial natural sources over the land area of China alone (see following section). The global annual mean mole fractions of $CHCl_3$ also show a similar trend to global emissions and emissions in China (Supplementary Fig. S9, derived from Laube and Tegtmeier et al.[2]), i.e., increasing through 2017 and then decreasing. The variation in the Northern Hemispheric mean mole fraction has largely mirrored that of the global mean, while the mole fractions in the Southern Hemisphere have been comparably stable since 2011. Given the short atmospheric lifetime of $CHCl_3$, it also indicates the dominant role of Northern Hemispheric anthropogenic emissions in the changes of global $CHCl_3$, which supports our finding.

Bottom-up $CHCl_3$ emissions in China and source identification

To understand the source sectors that drive the changes in $CHCl_3$ emissions in China, a process-based bottom-up inventory for $CHCl_3$ emissions in China was compiled for the first time using up-to-date data representative of applications which release $CHCl_3$. The bottom-up inventory considers both anthropogenic sources and natural sources (see Methods for details). The anthropogenic emission source sectors are listed in Fig. 1,

406 which includes intended anthropogenic emissions and by-product anthropogenic
407 emissions. The bottom-up inventory emissions (Fig. 3) show an increasing trend over
408 2011-2019, from 72 (58-86) Gg yr^{-1} in 2006 to 110 (87-131) Gg yr^{-1} in 2019, then a
409 decrease to 104 (84-126) Gg yr^{-1} in 2020. The bottom-up emissions in this study are
410 higher than previously derived emissions using an inter-species correlation method[60-62],
411 although emissions derived using inter-species correlation can be highly uncertain (Fig.
412 3a). The bottom-up emissions are also higher than a previous top-down $CHCl_3$
413 emissions from eastern China between 2007 and 2015[9], suggesting substantial
414 emissions outside of the eastern China region, while the top-down emissions in this
415 study for eastern China are of a similar magnitude to those found in the previous study[9]
416 over 2011-2015 (Supplementary Fig. S10). Our bottom-up emissions agree well with a
417 previous top-down emissions estimate for China in 2007[26] (Fig. 3a).

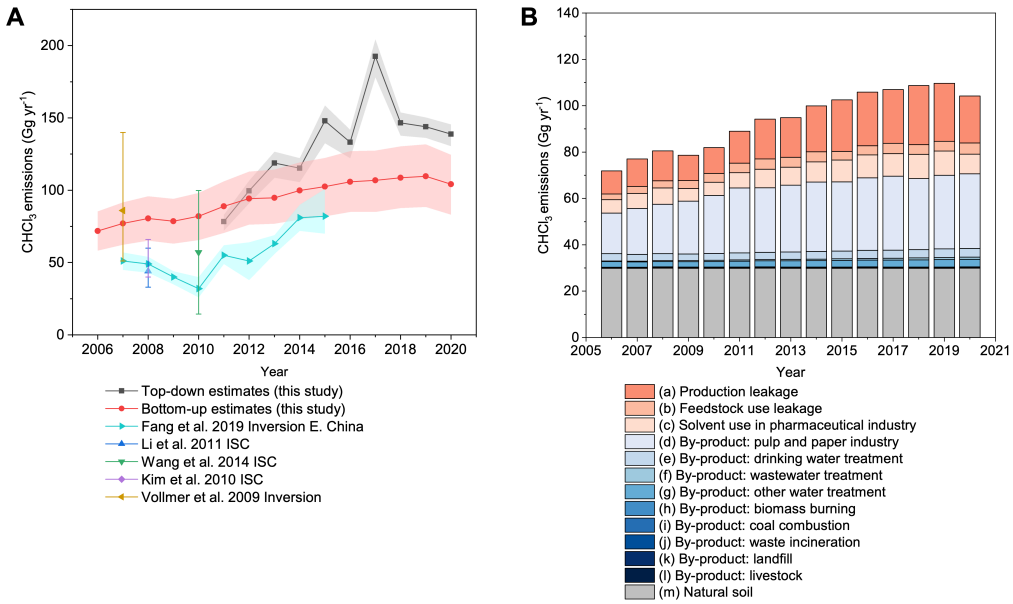

418

419 ***Fig. 3 Bottom-up and top-down $CHCl_3$ emissions in China. (A)*** *A comparison of the*
420 *top-down and bottom-up emissions in China derived in this study and from previous*

studies. The previous results include top-down emissions from Fang et al.[9], Li et al.[60], Wang et al.[61], Kim et al.[62] and Vollmer et al.[26]. The results from Fang et al.[9] only include $CHCl_3$ emissions from eastern China. ISC means emissions derived using an inter-species correlation method. ***(B)*** *Stacked sectoral emissions of the bottom-up results. The definition for each category can be found in the Methods. Sectoral emissions with uncertainties are shown in Supplementary Data file 4.*

Anthropogenic sources dominate the $CHCl_3$ emissions in China (Fig. 3b), accounting for ~68% of the overall emissions (averaged throughout the period). The largest anthropogenic source is by-product emissions of $CHCl_3$ from the pulp and paper sector, contributing ~20-35% to total bottom-up emissions, where $CHCl_3$ can be released during disinfecting or bleaching via haloform reaction when using chlorine-containing bleach[15,16]. The important role of the pulp and paper sector for $CHCl_3$ emissions is consistent with the conclusion from a previous global inventory[15]. This sector also contributed substantially to the increase during 2006-2019 in the bottom-up inventory, accounting for ~38% of the emissions increase. Production leakage is the second largest anthropogenic source, contributing ~10-25% to the overall emissions. This includes $CHCl_3$ emissions from several production-related processes such as $CHCl_3$ production, transport and storage. The production leakage sector contributes most to the increase during 2006-2019 (~40%) and the decrease during 2019-2020 (~87%) in the bottom-up inventory. The variation in $CHCl_3$ emissions from production leakage is driven by the rapid increase and decrease in $CHCl_3$ production in China ($CHCl_3$ production in China is shown in Supplementary Fig. S11), because a constant emission factor for

443 production leakage was used throughout. The solvent use of $CHCl_3$ in the
444 pharmaceutical industry also contributes substantially to overall bottom-up emissions
445 (~5-10%), to the 2006-2019 emission increase (~12%) and the 2019-2020 decrease
446 (~36%).

447 In addition to the anthropogenic emissions, previous studies reported relatively
448 uncertain but substantial contributions of natural sources to global $CHCl_3$ emissions,
449 ranging from ~50% to 90%[16-19], where terrestrial and ocean sources are thought to be
450 of similar magnitude[16,17]. In this study, the derived $CHCl_3$ emissions from natural soil
451 sources (representing the terrestrial emissions) account for ~32% (averaged throughout
452 the period) of the bottom-up emissions in China (Fig. 3b). As we only consider
453 emissions from land, no oceanic emissions of $CHCl_3$ in China are included.

454 The bottom-up emissions estimates in this study account for ~55-115% of the top-down
455 mean emissions estimates. There are substantial discrepancies between the top-down
456 and bottom-up emissions in 2015 and 2017. The large year-to-year variation in the top-
457 down emission estimates, including the temporary decrease in 2016 and the post-2017
458 decrease (Fig. 3a), are not well explained by the bottom-up emission estimates. The
459 top-down emissions are robust in terms of the sensitivity tests (Supplementary Fig. S3-
460 6), the substantial improvement of fitness to observations (Supplementary Table S2)
461 and error reductions (Supplementary Data file 2, >80% for annual national total in all
462 years). The mismatch between the top-down and bottom-up estimates may be caused
463 by many of the unknowns (like the potential emissions from the chlor-alkali industry

464 discussed in the next section) or uncertainties in the bottom-up inventory due to the
465 limitation in the availability of activity data or emission factors in several sectors.

466 The reported uncertainties in the bottom-up inventory are large enough that they could
467 encapsulate some of the year-to-year variability seen in the top-down estimates. Most
468 of the uncertainties in the inventory come from production leakage, the pulp and paper
469 industry, solvent use in pharmaceutical industry and natural soil sources
470 (Supplementary Data file 4). The bottom-up inventory does not explicitly include time-
471 varying emissions factors, e.g., a constant range of emission factors was used
472 throughout the period for production leakage (0.5-4%) and pulp and paper industry
473 (5.3×10^{-5}-4.54×10^{-4} g/g paper). However, year-to-year changes in these factors are
474 possible. For example, a decrease in the emission factors in the pulp and paper industry
475 (in terms of emissions per gram of paper) may result from increasing use of chlorine-
476 free bleach[63,64], and a possible decrease in emission factors for production leakage may
477 be due to actions to control pollutants from factories (e.g. ref.[65] which came into force
478 in 2017) in order to meet the 2017 target of the Air Pollution Prevention and Control
479 Action Plan in China[66]. If the entire uncertainty range of the production leakage rate
480 from the IPCC 2019 guidelines[42] was considered, which allows higher leakage rates
481 (see Supplementary Fig. S7 for details), the year-to-year variation in the top-down
482 estimates could be explained by uncertainties in the bottom-up estimates. Further
483 potential changes could be due to a sharp decrease in the volume of pharmaceutical
484 production in China after 2017[46] (see Supplementary Fig. S11 for details), where $CHCl_3$
485 is used as a solvent during pharmaceutical manufacturing.

In addition to potential unaccounted-for changes in anthropogenic emissions, it is possible that our bottom-up model has not accounted for substantial changes in natural emissions, as no time-varying and land type-dependent emissions factors were included. A negative correlation between the top-down emissions in China and annual average precipitation[67], especially after 2015 (Pearson Correlation Coefficient 'r' is -0.59, $p<0.001$ for ANOVA), and a positive correlation for the annual average temperature[67] and the emissions ($r=0.77$, $p<0.001$ for ANOVA), were identified (Supplementary Fig. S12). Extreme rainfall events in China in 2016[67] may be part of the explanation for the low emissions in 2016, as flooded conditions could sharply reduce $CHCl_3$ emission rates from soil[68]. High temperatures also have the potential to enhance the release of $CHCl_3$[69]. China only accounts for a minor fraction of global land area. Therefore, potential changes in natural emissions happening over the land area of China cannot explain the entire global emission changes and are unlikely to be the main cause for the global year-to-year variation.

Spatial distribution of $CHCl_3$ emissions in China and source identification

From examination of the spatial distribution of $CHCl_3$ emissions in China derived from atmospheric observations (shown in Fig. 4), most of the emission hotspots are in northern and eastern China. Provincial and regional emissions for each year are provided in Supplementary Data file 3 and Supplementary Fig. S13. North and East China (the definitions for each region can be found in Supplementary Fig. S13), including Hebei, Inner Mongolia, Shandong and Jiangsu provinces, have high

emissions compared to other regions throughout the study period. These regions are also among the highest contributors to the pre-2017 emissions increase and post-2017 decrease (Fig. 4e-f). North and East China are highly economically developed and industrialized regions, indicating the dominant role of anthropogenic sources in $CHCl_3$ emissions in China. Although the error reductions for emissions in North and East China show a slight decrease in 2017 compared to other years, when emissions in the years show a notable increase, they remain substantial (>65% uncertainty reductions in the regions). The error reduction from South China shows a minimum value in 2015 (58%), probably due to the lack of measurement sites in South China in this period. This may lead to larger uncertainty in emissions in 2015 but does not make much difference to the mean magnitudes and overall trends of overall emissions in China (see sensitivity tests in Supplementary Fig. S4-5).

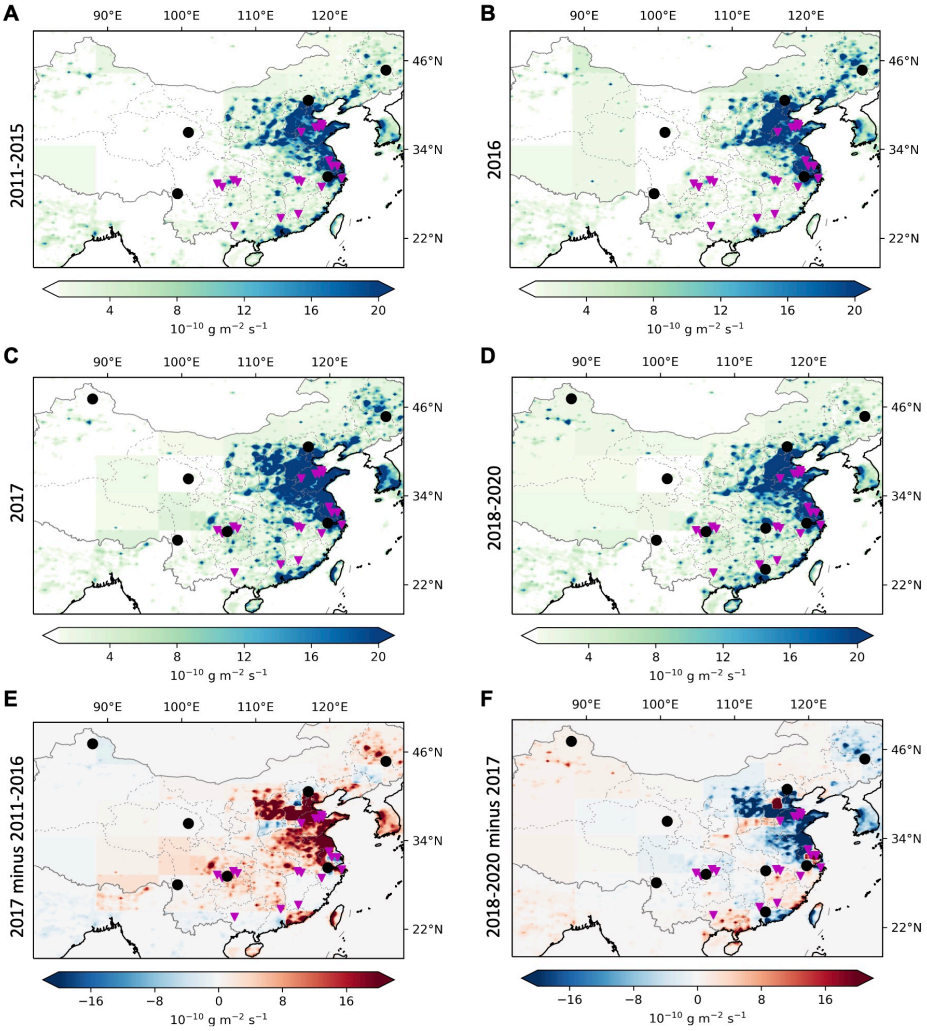

519

520 ***Fig. 4 Spatial distributions of $CHCl_3$ emissions in China.*** ***(A)*** *The mean posteriori*
521 *emissions over 2011-2015.* ***(B)*** *The mean posteriori emissions in 2016.* ***(C)*** *The mean*
522 *posteriori emissions in 2017.* ***(D)*** *The mean posteriori emissions over 2018-2020.* ***(E)***
523 *The difference in spatial distribution between 2017 and the 2011-2016 average (i.e.,*
524 *2017 minus the average of 2011-2016).* ***(F)*** *The difference in spatial distribution*
525 *between the 2018-2020 average and 2017 (i.e., the average of 2018-2020 minus 2017).*
526 *The time periods are divided to show the period before and after the maximum*
527 *emissions year in 2017 (pre-2017 increase and post-2017 decrease). The quantitative*
528 *provincial and regional emissions for each year are provided in Supplementary Data*

file 3 and Supplementary Fig. S13. The spatial distributions of the mean posteriori emissions in each individual year are shown in Supplementary Fig. S14. The black dots in the figures are the measurement sites active in the period. The pink triangles are the known chloromethane factories in China, some of which are also the main fluorine chemical factories in China producing HCFC-22 (where $CHCl_3$ is used as a feedstock).

The locations of some regions with high emissions are consistent with the locations of major chloromethane factories (mainly located in Shandong Province (in East China), the Yangtze River Delta region (in East China) and the Sichuan Basin (approximately at 103-108º E, 28-32º N), see Fig. 4), where fugitive emissions of chloromethanes have previously been identified[43,70,71]. Significant leakage of $CHCl_3$ from chloromethane factories during processes such as production, storage, or transport, identified by the bottom-up inventory in this study, are thus a likely source of emissions. The existence of high emissions in the Sichuan Basin region surrounding the Jiangjin (JGJ) site since 2017 also indicates the potential for emissions from chloromethanes factories (see Supplementary Fig. S14-15 for details), while the decrease in emissions in the Sichuan Basin during 2017-2020 (Fig. 4f) may be evidence for a decrease in the emission factor for production leakage from chloromethane factories. It is worth noting that the model-measurement errors for JGJ were large (Supplementary Fig. S8), possibly due to the relative complex meteorological conditions in the Basin.

There are similar spatial distribution patterns between $CHCl_3$ emissions (Fig. 4) and the pulp and paper industry and the pharmaceutical industry (Supplementary Fig. S16a-b).

There are no chloromethane factories in Hebei province (in North China), although the emissions in Hebei are substantial, especially in 2016 and 2018-2020 when Hebei is the province with the largest emissions (Supplementary Data file 3). Hebei is one of the most industrialized provinces in China where there is substantial pulp and paper production and pharmaceutical production. High $CHCl_3$ emissions and large paper and pharmaceutical production are also co-located in Shandong and Jiangsu provinces (in Yangtze River Delta region) in East China.

There are substantial $CHCl_3$ emissions from Inner Mongolia (in North China) and Xinjiang (in Northwest China) provinces (Supplementary Data file 3), which are not highly populated or industrialized regions and have no chloromethane factories. However, there is substantial chlor-alkali production in Hebei, Inner Mongolia and Xinjiang provinces (Supplementary Fig. S16c). As chlor-alkali factories are regarded as potential sources for CCl_4 emissions[43,72], possibly via chlorination of organic substances, they could also be sources for $CHCl_3$ emissions as $CHCl_3$ is easily formed via haloform reactions during chlorination[15]. The emissions in the seven sub-regions (Supplementary Fig. S13) are strongly correlated (r=0.82) with caustic soda production in the regions[46] (Supplementary Fig. S17), which further indicates a potential link between chlor-alkali production and $CHCl_3$ emissions, although the exact process of $CHCl_3$ formation is unclear.

Discussion

A substantial increase in the global $CHCl_3$ mole fractions and emissions up to 2015 had

571 previously been identified and could have delayed the recovery of Antarctic
572 stratospheric ozone by up to 9 years if the increase continued (defined as the 'continued
573 growth scenario' in Fang et al.[9]). The increase in both global $CHCl_3$ mole fractions and
574 emissions was found to continue until 2017, but both were then followed by a fall in
575 2018[2]. The global emissions and mole fractions were approximately constant between
576 2019 and 2020, and the mole fractions in these years are similar to those in 2015 (Fig.
577 2 and Supplementary Fig. S9). This implies that the impact of $CHCl_3$ on global ozone
578 layer recovery may be close to the 'constant mole fraction scenario' in Fang et al.[9]. If
579 the plateau in mole fractions and emissions continues, the potential delay from $CHCl_3$
580 on Antarctic stratospheric ozone recovery should be ~1 year when the total increase in
581 $CHCl_3$ mole fraction since 1920 was considered[9]. Thus, a significant delay in the
582 recovery of the ozone layer caused by the increasing $CHCl_3$ emissions could be avoided
583 if future $CHCl_3$ emissions do not increase.

584 The predicted future trajectory for $CHCl_3$ emissions is uncertain. The changes in global
585 $CHCl_3$ emissions have likely been dominated by emission changes from anthropogenic
586 sources in China between 2011 and 2020. By-product emissions during bleaching in
587 the pulp and paper industry, production leakage from the chloromethane industry and
588 emissions from solvent use in the pharmaceutical industry are recognized as important
589 sources of $CHCl_3$ emissions in China in our analyses. The year-to-year variations in
590 emissions from China and the differences between top-down and bottom-up emissions
591 may be reconciled by several uncertainties in anthropogenic emissions in the bottom-
592 up inventory, such as the lack of time-varying emissions factors for production leakage

593 and the pulp and paper industry, and the lack of quantification of emissions in the chlor-
594 alkali industry. However, the lack of available data limit further exploration of these
595 uncertainties. Further efforts, like carrying out high-frequency measurements in key
596 areas and samplings around important industries[71] would offer a better understanding
597 of these uncertainties. Natural soil emissions are likely to be substantial in China
598 (~32%), as identified from the bottom-up inventory, and have potential interannual
599 variations related to the changes in annual temperature and precipitation. However, they
600 are not likely to be the main cause for the global emission changes considering the size
601 of China's land and global ocean emissions.

602 Most of the identified major anthropogenic sources of $CHCl_3$ in China can be controlled
603 effectively by measures such as applying chlorine-free bleach in the pulp and paper
604 industry or imposing stricter regulations on production leakage. These measures could
605 help maintain or reduce $CHCl_3$ emissions, to further mitigate the impacts of $CHCl_3$ on
606 the ozone layer. Even though the long-term impact on ozone layer recovery from $CHCl_3$
607 has been reduced due to the fall in emissions in recent years, its cumulative increased
608 emissions over 2011-2020 have already caused an integrated ozone depletion
609 comparable to that of increased CFC-11 emissions since 2012[8] which have
610 subsequently decreased since 2018 (see Supplementary Text S1). Considering the
611 increasing importance of $CHCl_3$ for ozone depletion compared to ozone depleting
612 substances controlled under the Montreal Protocol, and that $CHCl_3$ emissions in East
613 Asia can be rapidly transported into the stratosphere, an improved understanding of its
614 sources in China is needed, to better understand the future evolution of stratospheric

615 ozone.

Data availability

Measurement data of $CHCl_3$ from the Chinese network are provided in the Supplementary Data file 1. Use of the Chinese measurement data in publications, reports or presentations requires the users to contact B.Y. (yaobo@fudan.edu.cn) first to discuss your interests.

Code availability

The code for the regional emission inversion framework is available at https://github.com/ACRG-Bristol/acrg (https://doi.org/10.5281/zenodo.6834888, Rigby et al., 2022*), and all relevant inputs and outputs are available upon request from M.A. (mindean@mit.edu). License to use NAME is available upon request to the UK Met Office (enquiries@metoffice.gov.uk).

*Rigby, M. et al. ACRG-Bristol/acrg: ACRG v0.2.0 (v0.2.0), Zenodo [code], https://doi.org/10.5281/zenodo.6834888, 2022.

Author Contributions

M.A. designed the research. M.A. conducted the regional inverse modelling and interpreted the results with the support of L.M.W., M.R. and A.L.G.. B.Y. provided measurement data from the nine CMA sites and P.B.K., J.M., S.O'D., R.G.P., R.F.W. and D.Y. provided global measurement data and calibrations. R.H. provided a priori boundary condition values. M.A. led the writing of the manuscript, with contributions from L.M.W., J.H., B.Y., M.R., J.M., A.L.G., R.G.P. and all other authors.

Acknowledgements

This work was supported by the National Key Research and Development Program of China (Grant No. 2019YFC0214500) and Shanghai B&R Joint Laboratory Project (No. 22230750300). This work has benefited from the technical expertise of and the assistance by the AGAGE (Advanced Global Atmospheric Gases Experiment) network including the Medusa GC/MS system technology, calibrations of $CHCl_3$ measurements and network operation, as well as Dr. Martin Vollmer from the Swiss Federal Laboratories for Materials Science and Technology. Ronald Prinn, Minde An, Jens Mühle, Paul Krummel, Simon O'Doherty, Ray Weiss and Dickon Young acknowledge AGAGE support via NASA (USA) grants to MIT (with sub-awards to Bristol University, and CSIRO) and to SIO (including AGAGE calibration). Luke M. Western received funding from the European Union's Horizon 2020 research and innovation programme under Marie Skłodowska-Curie grant agreement no. 101030750. We acknowledge the support from members of Atmospheric Chemistry Research Group at University of Bristol and thank the U.K. Met Office for the support and licensing for NAME.

Supporting Information Available

Supplementary Information: Text S1, Figures S1-S17 and Tables S1-S5 (PDF)

Supplementary Data 1: Raw observed $CHCl_3$ mole fractions from nine Chinese sites used in the regional emission inversion framework (XLSX)

Supplementary Data 2: Error reductions of the inverse modellings with different a priori

probability distributions (XLSX).

Supplementary Data 3: Derived top-down $CHCl_3$ emissions in China (XLSX)

Supplementary Data 4: Sectoral bottom-up $CHCl_3$ emission inventory in China (XLSX)

This information is available free of charge via the Internet at http://pubs.acs.org.

Competing Interests

The authors declare no competing interests.

References

(1) Solomon, S.; Ivy, D. J.; Kinnison, D.; Mills, M. J.; Neely, R. R.; Schmidt, A. Emergence of Healing in the Antarctic Ozone Layer. Science 2016, 353 (6296), 269-274.

(2) Laube, J. C.; Tegtmeier, S. Chapter 1: Update on Ozone-Depleting Substances (ODSs) and Other Gases of Interest to the Montreal Protocol. In Scientific Assessment of Ozone Depletion: 2022; World Meteorological Organization: Geneva, Switzerland, 2022; Vol. 278.

(3) Oram, D. E.; Ashfold, M. J.; Laube, J. C.; Gooch, L. J.; Humphrey, S.; Sturges, W. T.; Leedham-Elvidge, E.; Forster, G. L.; Harris, N. R. P.; Mead, M. I.; Samah, A. A.; Phang, S. M.; Ou-Yang, C.-F.; Lin, N.-H.; Wang, J.-L.; Baker, A. K.; Brenninkmeijer, C. A. M.; Sherry, D. A Growing Threat to the Ozone Layer from Short-Lived Anthropogenic Chlorocarbons. Atmos. Chem. Phys. 2017, 17 (19), 11929-11941.

(4) Hossaini, R.; Chipperfield, M. P.; Montzka, S. A.; Leeson, A. A.; Dhomse, S. S.; Pyle, J. A. The Increasing Threat to Stratospheric Ozone from Dichloromethane. Nat. Commun. 2017, 8, 15962.

(5) Randel, W. J.; Park, M.; Emmons, L.; Kinnison, D.; Bernath, P.; Walker, K. A.; Boone, C.; Pumphrey, H. Asian Monsoon Transport of Pollution to the Stratosphere. Science 2010, 328 (5978), 611-613.

(6) Claxton, T.; Hossaini, R.; Wild, O.; Chipperfield, M. P.; Wilson, C. On the Regional and Seasonal Ozone Depletion Potential of Chlorinated Very Short-lived Substances. Geophys. Res. Lett. 2019, 46 (10), 5489-5498.

(7) Ashfold, M. J.; Pyle, J. A.; Robinson, A. D.; Meneguz, E.; Nadzir, M. S. M.; Phang, S. M.; Samah, A. A.; Ong, S.; Ung, H. E.; Peng, L. K.; Yong, S. E.; Harris, N. R.

P. Rapid Transport of East Asian Pollution to the Deep Tropics. Atmos. Chem. Phys. 2015, 15 (6), 3565-3573.

(8) Pyle, J. A.; Keeble, J.; Abraham, N. L.; Chipperfield, M. P.; Griffiths, P. T. Integrated Ozone Depletion as a Metric for Ozone Recovery. Nature 2022, 608 (7924), 719-723.

(9) Fang, X.; Park, S.; Saito, T.; Tunnicliffe, R.; Ganesan, A. L.; Rigby, M.; Li, S.; Yokouchi, Y.; Fraser, P. J.; Harth, C. M.; Krummel, P. B.; Mühle, J.; O'Doherty, S.; Salameh, P. K.; Simmonds, P. G.; Weiss, R. F.; Young, D.; Lunt, M. F.; Manning, A. J.; Gressent, A.; Prinn, R. G. Rapid Increase in Ozone-Depleting Chloroform Emissions from China. Nat. Geosci. 2019, 12 (2), 89-93.

(10) Dhomse, S. S.; Feng, W.; Montzka, S. A.; Hossaini, R.; Keeble, J.; Pyle, J. A.; Daniel, J. S.; Chipperfield, M. P. Delay in Recovery of the Antarctic Ozone Hole from Unexpected CFC-11 Emissions. Nat. Commun. 2019, 10 (1), 5781.

(11) Fleming, E. L.; Newman, P. A.; Liang, Q.; Daniel, J. S. The Impact of Continuing CFC-11 Emissions on Stratospheric Ozone. J. Geophys. Res. Atmos. 2020, 125 (3).

(12) China Chlor-Alkali Industry Association (CCAIA). Report on Chloromethanes Industry in China (in Chinese), 2021. http://www.ccaon.com/jwlhw.asp.

(13) Bie, P.; Fang, X.; Li, Z.; Wang, Z.; Hu, J. Emissions Estimates of Carbon Tetrachloride for 1992-2014 in China. Environ. Pollut. 2017, 224, 670-678.

(14) Feng, Y.; Bie, P.; Wang, Z.; Wang, L.; Zhang, J. Bottom-up Anthropogenic Dichloromethane Emission Estimates from China for the Period 2005-2016 and Predictions of Future Emissions. Atmos. Environ. 2018, 186, 241-247.

(15) Aucott, M. L.; McCulloch, A.; Graedel, T. E.; Kleiman, G.; Midgley, P.; Li, Y.-F. Anthropogenic Emissions of Trichloromethane (Chloroform, $CHCl_3$) and Chlorodifluoromethane (HCFC-22): Reactive Chlorine Emissions Inventory. J. Geophys. Res. Atmos. 1999, 104 (D7), 8405-8415.

(16) McCulloch, A. Chloroform in the Environment: Occurrence, Sources, Sinks and Effects. Chemosphere 2003, 50 (10), 1291-1308.

(17) Cox, M. L.; Sturrock, G. A.; Fraser, P. J.; Siems, S. T.; Krummel, P. B.; O'Doherty, S. Regional Sources of Methyl Chloride, Chloroform and Dichloromethane Identified from AGAGE Observations at Cape Grim, Tasmania, 1998-2000. J. Atmos. Chem. 2003, 45 (1), 79-99.

(18) Trudinger, C. M.; Etheridge, D. M.; Sturrock, G. A.; Fraser, P. J.; Krummel, P. B.; McCulloch, A. Atmospheric Histories of Halocarbons from Analysis of Antarctic Firn Air: Methyl Bromide, Methyl Chloride, Chloroform, and Dichloromethane. J. Geophys. Res. Atmos. 2004, 109 (D22), D22310.

(19) Worton, D. R.; Sturges, W. T.; Schwander, J.; Mulvaney, R.; Barnola, J. M.;

Chappellaz, J. 20th Century Trends and Budget Implications of Chloroform and Related Tri-and Dihalomethanes Inferred from Firn Air. Atmos. Chem. Phys. 2006, 6 (10), 2847-2863.

(20) Brioude, J.; Portmann, R. W.; Daniel, J. S.; Cooper, O. R.; Frost, G. J.; Rosenlof, K. H.; Granier, C.; Ravishankara, A. R.; Montzka, S. A.; Stohl, A. Variations in Ozone Depletion Potentials of Very Short-Lived Substances with Season and Emission Region. Geophys. Res. Lett. 2010, 37 (19), L19804.

(21) An, M.; Western, L. M.; Say, D.; Chen, L.; Claxton, T.; Ganesan, A. L.; Hossaini, R.; Krummel, P. B.; Manning, A. J.; Mühle, J.; O'Doherty, S.; Prinn, R. G.; Weiss, R. F.; Young, D.; Hu, J.; Yao, B.; Rigby, M. Rapid Increase in Dichloromethane Emissions from China Inferred through Atmospheric Observations. Nat. Commun. 2021, 12 (1), 7279.

(22) Zhang, G.; Yao, B.; Vollmer, M. K.; Montzka, S. A.; Mühle, J.; Weiss, R. F.; O'Doherty, S.; Li, Y.; Fang, S.; Reimann, S. Ambient Mixing Ratios of Atmospheric Halogenated Compounds at Five Background Stations in China. Atmos. Environ. 2017, 160, 55-69.

(23) Yu, D.; Yao, B.; Lin, W.; Vollmer, M. K.; Ge, B.; Zhang, G.; Li, Y.; Xu, H.; O'Doherty, S.; Chen, L.; Reimann, S. Atmospheric CH_3CCl_3 Observations in China: Historical Trends and Implications. Atmos. Res. 2020, 231, 104658.

(24) Arnold, T.; Mühle, J.; Salameh, P. K.; Harth, C. M.; Ivy, D. J.; Weiss, R. F. Automated Measurement of Nitrogen Trifluoride in Ambient Air. Anal. Chem. 2012, 84 (11), 4798-4804.

(25) Miller, B. R.; Weiss, R. F.; Salameh, P. K.; Tanhua, T.; Greally, B. R.; Mühle, J.; Simmonds, P. G. Medusa: A Sample Preconcentration and GC/MS Detector System for in Situ Measurements of Atmospheric Trace Halocarbons, Hydrocarbons, and Sulfur Compounds. Anal. Chem. 2008, 80 (5), 1536-1545.

(26) Vollmer, M. K.; Zhou, L. X.; Greally, B. R.; Henne, S.; Yao, B.; Reimann, S.; Stordal, F.; Cunnold, D. M.; Zhang, X. C.; Maione, M.; Zhang, F.; Huang, J.; Simmonds, P. G. Emissions of Ozone-Depleting Halocarbons from China. Geophys. Res. Lett. 2009, 36 (15), L15823.

(27) Prinn, R. G.; Weiss, R. F.; Arduini, J.; Arnold, T.; DeWitt, H. L.; Fraser, P. J.; Ganesan, A. L.; Gasore, J.; Harth, C. M.; Hermansen, O.; Kim, J.; Krummel, P. B.; Li, S.; Loh, Z. M.; Lunder, C. R.; Maione, M.; Manning, A. J.; Miller, B. R.; Mitrevski, B.; Mühle, J.; O'Doherty, S.; Park, S.; Reimann, S.; Rigby, M.; Saito, T.; Salameh, P. K.; Schmidt, R.; Simmonds, P. G.; Steele, L. P.; Vollmer, M. K.; Wang, R. H.; Yao, B.; Yokouchi, Y.; Young, D.; Zhou, L. History of Chemically and Radiatively Important Atmospheric Gases from the Advanced Global Atmospheric Gases Experiment (AGAGE). Earth Syst. Sci. Data 2018, 10 (2), 985-1018.

(28) Lunt, M. F.; Rigby, M.; Ganesan, A. L.; Manning, A. J. Estimation of Trace Gas

Fluxes with Objectively Determined Basis Functions Using Reversible-Jump Markov Chain Monte Carlo. Geosci. Model Dev. 2016, 9 (9), 3213-3229.

(29) Ganesan, A. L.; Rigby, M.; Zammit-Mangion, A.; Manning, A. J.; Prinn, R. G.; Fraser, P. J.; Harth, C. M.; Kim, K.-R.; Krummel, P. B.; Li, S.; Mühle, J.; O'Doherty, S. J.; Park, S.; Salameh, P. K.; Steele, L. P.; Weiss, R. F. Characterization of Uncertainties in Atmospheric Trace Gas Inversions Using Hierarchical Bayesian Methods. Atmos. Chem. Phys. 2014, 14 (8), 3855-3864.

(30) Rigby, M.; Park, S.; Saito, T.; Western, L. M.; Redington, A. L.; Fang, X.; Henne, S.; Manning, A. J.; Prinn, R. G.; Dutton, G. S.; Fraser, P. J.; Ganesan, A. L.; Hall, B. D.; Harth, C. M.; Kim, J.; Kim, K. R.; Krummel, P. B.; Lee, T.; Li, S.; Liang, Q.; Lunt, M. F.; Montzka, S. A.; Muhle, J.; O'Doherty, S.; Park, M. K.; Reimann, S.; Salameh, P. K.; Simmonds, P.; Tunnicliffe, R. L.; Weiss, R. F.; Yokouchi, Y.; Young, D. Increase in CFC-11 Emissions from Eastern China Based on Atmospheric Observations. Nature 2019, 569 (7757), 546-550.

(31) Park, S.; Western, L. M.; Saito, T.; Redington, A. L.; Henne, S.; Fang, X.; Prinn, R. G.; Manning, A. J.; Montzka, S. A.; Fraser, P. J.; Ganesan, A. L.; Harth, C. M.; Kim, J.; Krummel, P. B.; Liang, Q.; Mühle, J.; O'Doherty, S.; Park, H.; Park, M.-K.; Reimann, S.; Salameh, P. K.; Weiss, R. F.; Rigby, M. A Decline in Emissions of CFC-11 and Related Chemicals from Eastern China. Nature 2021, 590 (7846), 433-437.

(32) Jones, A.; Thomson, D.; Hort, M.; Devenish, B. The U.K. Met Office's Next-Generation Atmospheric Dispersion Model, NAME III. In Air Pollution Modeling and Its Application XVII; Borrego, C., Norman, A.-L., Eds.; Springer US, Boston, MA: Boston, MA, 2007; pp 580-589.

(33) Say, D.; Kuyper, B.; Western, L.; Khan, M. A. H.; Lesch, T.; Labuschagne, C.; Martin, D.; Young, D.; Manning, A. J.; O'Doherty, S.; Rigby, M.; Krummel, P. B.; Davies-Coleman, M. T.; Ganesan, A. L.; Shallcross, D. E. Emissions and Marine Boundary Layer Concentrations of Unregulated Chlorocarbons Measured at Cape Point, South Africa. Environ. Sci. Technol. 2020, 54 (17), 10514-10523.

(34) Western, L. M.; Redington, A. L.; Manning, A. J.; Trudinger, C. M.; Hu, L.; Henne, S.; Fang, X.; Kuijpers, L. J. M.; Theodoridi, C.; Godwin, D. S.; Arduini, J.; Dunse, B.; Engel, A.; Fraser, P. J.; Harth, C. M.; Krummel, P. B.; Maione, M.; Mühle, J.; O'Doherty, S.; Park, H.; Park, S.; Reimann, S.; Salameh, P. K.; Say, D.; Schmidt, R.; Schuck, T.; Siso, C.; Stanley, K. M.; Vimont, I.; Vollmer, M. K.; Young, D.; Prinn, R. G.; Weiss, R. F.; Montzka, S. A.; Rigby, M. A Renewed Rise in Global HCFC-141b Emissions between 2017-2021. Atmos. Chem. Phys. 2022, 22 (14), 9601-9616.

(35) Walters, D.; Baran, A. J.; Boutle, I.; Brooks, M.; Earnshaw, P.; Edwards, J.; Furtado, K.; Hill, P.; Lock, A.; Manners, J.; Morcrette, C.; Mulcahy, J.; Sanchez, C.; Smith, C.; Stratton, R.; Tennant, W.; Tomassini, L.; Van Weverberg, K.; Vosper, S.; Willett, M.; Browse, J.; Bushell, A.; Carslaw, K.; Dalvi, M.; Essery, R.; Gedney,

N.; Hardiman, S.; Johnson, B.; Johnson, C.; Jones, A.; Jones, C.; Mann, G.; Milton, S.; Rumbold, H.; Sellar, A.; Ujiie, M.; Whitall, M.; Williams, K.; Zerroukat, M. The Met Office Unified Model Global Atmosphere 7.0/7.1 and JULES Global Land 7.0 Configurations. Geosci. Model Dev. 2019, 12 (5), 1909-1963.

(36) Hoffman, M. D.; Gelman, A. The No-U-Turn Sampler: Adaptively Setting Path Lengths in Hamiltonian Monte Carlo. J. Mach. Learn. Res. 2014, 15, 1593-1623.

(37) Neal, R. M. Slice Sampling. Ann. Stat. 2003, 31 (3), 705-767.

(38) Monks, S. A.; Arnold, S. R.; Hollaway, M. J.; Pope, R. J.; Wilson, C.; Feng, W.; Emmerson, K. M.; Kerridge, B. J.; Latter, B. L.; Miles, G. M.; Siddans, R.; Chipperfield, M. P. The TOMCAT Global Chemical Transport Model v1.6: Description of Chemical Mechanism and Model Evaluation. Geosci. Model Dev. 2017, 10 (8), 3025-3057.

(39) Finkel, R. A.; Bentley, J. L. Quad Trees a Data Structure for Retrieval on Composite Keys. Acta Inform. 1974, 4 (1), 1-9.

(40) General Administration of Customs of China. China Customs Statistical Yearbook (in Chinese); China Customs Press, Beijing, China: Beijing, China, 2020.

(41) Intergovernmental Panel on Climate Change (IPCC). Good Practice Guidance and Uncertainty Management in National Greenhouse Gas Inventories; IPCC, Japan: Japan, 2000.

(42) Intergovernmental Panel on Climate Change (IPCC). 2019 Refinement to the 2006 IPCC Guidelines for National Greenhouse Gas Inventories; IPCC, Switzerland: Switzerland, 2019.

(43) Sherry, D.; McCulloch, A.; Liang, Q.; Reimann, S.; Newman, P. A. Current Sources of Carbon Tetrachloride (CCl_4) in Our Atmosphere. Environ. Res. Lett. 2018, 13 (2), 024004.

(44) Zhao, X.-C.; Xiang, X.-Y.; Wang, S.-C.; Jiang, P.-N.; Gao, D.; Yi, L.-Y.; An, M.-D.; Bai, F.-L.; Xu, W.-G.; Zhang, J.-J.; Hu, J.-X. By-Production, Emissions and Abatement Cost-Climate Benefit of HFC-23 in China's HCFC-22 Plants. Adv. Clim. Change Res. 2023, S1674927823000126.

(45) United States Environmental Protection Agency (USEPA). Locating and Estimating Air Emissions from Sources of Chloroform, 1984. https://www.epa.gov/sites/default/files/2020-11/documents/chloroform.pdf (accessed 2022-12-29).

(46) National Bureau of Statistics of China. China Statistical Yearbook; China Statistics Press, Beijing, China: Beijing, China, 2021.

(47) Ministry of Housing and Urban-Rural Development of China. China Urban-Rural Construction Statistical Yearbook (in Chinese); China Statistics Press, Beijing, China: Beijing, China, 2020.

(48) Lobert, J. M.; Keene, W. C.; Logan, J. A.; Yevich, R. Global Chlorine Emissions from Biomass Burning: Reactive Chlorine Emissions Inventory. J. Geophys. Res. Atmos. 1999, 104 (D7), 8373-8389.

(49) Wu, J.; Kong, S.; Wu, F.; Cheng, Y.; Zheng, S.; Qin, S.; Liu, X.; Yan, Q.; Zheng, H.; Zheng, M.; Yan, Y.; Liu, D.; Ding, S.; Zhao, D.; Shen, G.; Zhao, T.; Qi, S. The Moving of High Emission for Biomass Burning in China: View from Multi-Year Emission Estimation and Human-Driven Forces. Environ. Int. 2020, 142, 105812.

(50) Department of Energy Statistics, National Bureau of Statistics. China Energy Statistical Yearbook (in Chinese); China Statistics Press, Beijing, China: Beijing, China, 2021.

(51) United States Environmental Protection Agency (USEPA). WebFIRE database. https://www.epa.gov/electronic-reporting-air-emissions/webfire (accessed 2022-02-25).

(52) Liu, Y.; Lu, W.; Dastyar, W.; Liu, Y.; Guo, H.; Fu, X.; Li, H.; Meng, R.; Zhao, M.; Wang, H. Fugitive Halocarbon Emissions from Working Face of Municipal Solid Waste Landfills in China. Waste Manag. 2017, 70, 149-157.

(53) Crippa, M.; Guizzardi, D.; Muntean, M.; Schaaf, E.; Lo Vullo, E.; Solazzo, E.; Monforti-Ferrario, F.; Olivier, J.; Vignati, E. EDGAR v7.0 Greenhouse Gas Emissions. https://edgar.jrc.ec.europa.eu/dataset_ghg70 (accessed 2022-12-25).

(54) Food and Agriculture Organization of the United Nations. FAOSTAT Greenhouse Gas Emissions Database. https://www.fao.org/faostat/en/#data/GT (accessed 2022-12-25).

(55) Chang, J.; Peng, S.; Yin, Y.; Ciais, P.; Havlik, P.; Herrero, M. The Key Role of Production Efficiency Changes in Livestock Methane Emission Mitigation. AGU Adv. 2021, 2 (2), e2021AV000391.

(56) Dimmer, C. H.; Simmonds, P. G.; Nickless, G.; Bassford, M. R. Biogenic Fluxes of Halomethanes from Irish Peatland Ecosystems. Atmos. Environ. 2001, 35 (2), 321-330.

(57) Laturnus, F.; Haselmann, K. F.; Borch, T.; Grøn, C. Terrestrial Natural Sources of Trichloromethane (Chloroform, $CHCl_3$)-an Overview. Biogeochemistry 2002, 60 (2), 121-139.

(58) Khalil, M. A. K.; Rasmussen, R. A.; Shearer, M. J.; Chen, Z.-L.; Yao, H.; Yang, J. Emissions of Methane, Nitrous Oxide, and Other Trace Gases from Rice Fields in China. J. Geophys. Res. Atmos. 1998, 103 (D19), 25241-25250.

(59) Khalil, M.; Moore, R.; Harper, D.; Lobert, J.; Erickson, D.; Koropalov, V.; Sturges, W.; Keene, W. Natural Emissions of Chlorine-containing Gases: Reactive Chlorine Emissions Inventory. J. Geophys. Res. Atmos. 1999, 104 (D7), 8333-8346.

(60) Li, S.; Kim, J.; Kim, K. R.; Muhle, J.; Kim, S. K.; Park, M. K.; Stohl, A.; Kang, D. J.; Arnold, T.; Harth, C. M.; Salameh, P. K.; Weiss, R. F. Emissions of Halogenated Compounds in East Asia Determined from Measurements at Jeju Island, Korea. Environ. Sci. Technol. 2011, 45 (13), 5668-5675.

(61) Wang, C.; Shao, M.; Huang, D.; Lu, S.; Zeng, L.; Hu, M.; Zhang, Q. Estimating Halocarbon Emissions Using Measured Ratio Relative to Tracers in China. Atmos. Environ. 2014, 89, 816-826.

(62) Kim, J.; Li, S.; Kim, K.-R.; Stohl, A.; Mühle, J.; Kim, S.-K.; Park, M.-K.; Kang, D.-J.; Lee, G.; Harth, C. M.; Salameh, P. K.; Weiss, R. F. Regional Atmospheric Emissions Determined from Measurements at Jeju Island, Korea: Halogenated Compounds from China. Geophys. Res. Lett. 2010, 37 (12), L12801.

(63) Wen, Z.; Di, J.; Zhang, X. Uncertainty Analysis of Primary Water Pollutant Control in China's Pulp and Paper Industry. J. Environ. Manage. 2016, 169, 67-77.

(64) Zhang, C.; Chen, J.; Wen, Z. Alternative Policy Assessment for Water Pollution Control in China's Pulp and Paper Industry. Resour. Conserv. Recycl. 2012, 66, 15-26.

(65) People's Government of Shandong Province. Action Plan for Comprehensive Control of Air Pollution in the Autumn and Winter of 2017-2018 in the Beijing-Tianjin-Hebei Region and Its Surrounding Areas (in Chinese), 2017. http://www.shandong.gov.cn/art/2017/9/27/art_2259_26171.html.

(66) The State Council of People's Republic of China. Air Pollution Prevention and Control Action Plan (in Chinese), 2013. http://www.gov.cn/zhengce/content/2013-09/13/content_4561.htm.

(67) China Meteorological Administration. China Climate Bulletin (in Chinese); 2021.

(68) Rhew, R. C.; Teh, Y. A.; Abel, T.; Atwood, A.; Mazéas, O. Chloroform Emissions from the Alaskan Arctic Tundra. Geophys. Res. Lett. 2008, 35 (21), L21811.

(69) Khalil, M. A. K.; Rasmussen, R. A.; French, J. R. J.; Holt, J. A. The Influence of Termites on Atmospheric Trace Gases: CH_4, CO_2, $CHCl_3$, N_2O, CO, H_2, and Light Hydrocarbons. J. Geophys. Res. 1990, 95 (D4), 3619.

(70) United Nations Environment Programme (UNEP). Report on Emission Reductions and Phase-out of CTC (Decision 55/45), 2009. UNEP/OzL.Pro/ExCom/58/50.

(71) Li, B.; Zhao, X.; Li, X.; Hu, X.; Hu, L.; Chen, D.; An, M.; Yang, Y.; Feng, R.; Guo, L.; Jiang, P.; Yao, B.; Hu, J.; Fang, X. Emission Factors of Ozone-Depleting Chloromethanes during Production Processes Based on Field Measurements Surrounding a Typical Chloromethane Plant in China. J. Clean. Prod. 2023, 414, 137573.

(72) Hu, L.; Montzka, S. A.; Miller, B. R.; Andrews, A. E.; Miller, J. B.; Lehman, S. J.; Sweeney, C.; Miller, S. M.; Thoning, K.; Siso, C.; Atlas, E. L.; Blake, D. R.; de Gouw, J.; Gilman, J. B.; Dutton, G.; Elkins, J. W.; Hall, B.; Chen, H.; Fischer, M. L.; Mountain, M. E.; Nehrkorn, T.; Biraud, S. C.; Moore, F. L.; Tans, P. Continued Emissions of Carbon Tetrachloride from the United States Nearly Two Decades after Its Phaseout for Dispersive Uses. Proc. Natl. Acad. Sci. 2016, 113 (11), 2880-2885.

928 **TOC:**

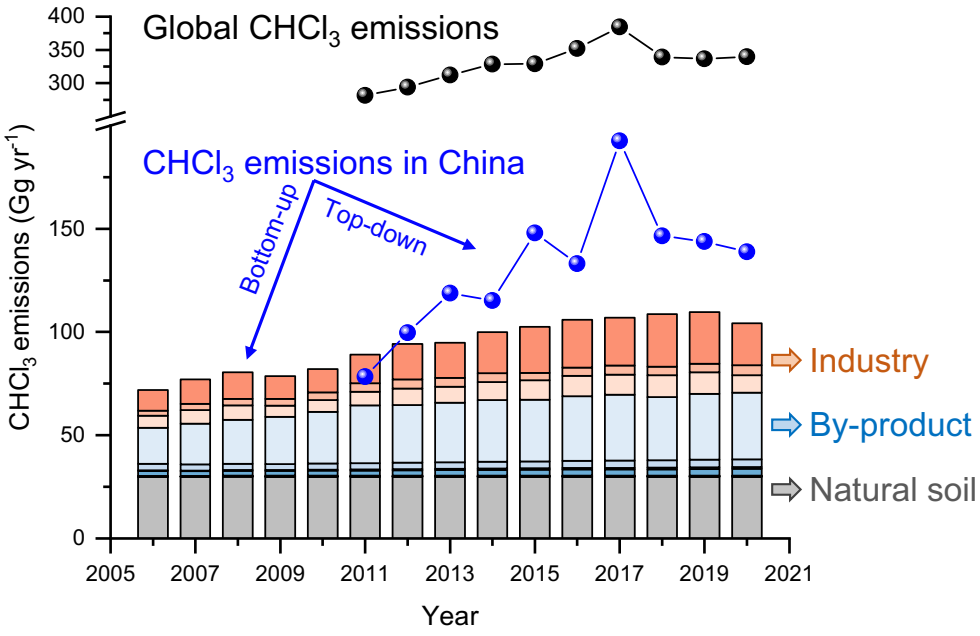
Global $CHCl_3$ emissions
$CHCl_3$ emissions in China
Bottom-up
Top-down
$CHCl_3$ emissions (Gg yr^{-1})
Year
Industry
By-product
Natural soil
400
350
300
150
100
50
0
2005
2007
2009
2011
2013
2015
2017
2019
2021

929